PAPER Nr.: 88

COMPUTATIONAL FLUID DYNAMICS 3-D ANALYSIS FOR ADVANCED TRANSONIC TURBINE DESIGN

S. Colantuoni, A. Colella, G. Santoriello

ALFA ROMEO AVIO S.p.A.
Research and Development
NAPOLI - ITALY

FIFTEENTH EUROPEAN ROTORCRAFT FORUM

SEPTEMBER 12-15, 1989 AMSTERDAM

COMPUTATIONAL FLUID DYNAMICS 3-D ANALYSIS FOR ADVANCED TRANSONIC TURBINE DESIGN

S. Colantuoni, A. Colella, G. Santoriello

ALFA ROMEO AVIO S.p.A.
NAPOLI - ITALY

ABSTRACT

Advanced small propulsion engines for today and year 2000 rotorcraft competitive applications require a design philosophy based on the fully integration of key-technology areas applied to critical components. Recent studies and consolidated results from most leader companies show that the a small high-loaded transonic axial turbine stage, capable of operating efficiently, under heavy thermal condition with sofisticated cooling sistem, is one of the main target for the high-tech core engine design.

A research program on the advanced design technology of high temperature turbine stages is ongoing at Alfa Romeo Avio. In the following paper, an overview of the most significative applications of the CFD 3-D inviscid method to the analysis of an existing transonic turbine stage is presented. The comparison between numerical results and first experimental detail measurements of the flowfield at NGV exit plane, obtained by a laser anemometry system on a cold-air turbine rig, is discussed.

1. INTRODUCTION

1.1 Requirements of future helicopter propulsion engines

Propulsion systems based on small gas-turbine engine are subject to expensive and time-consuming process of evolution, in order to satisfy the severe requirements of today and year 2000 helicopter market. Starting from the mission analysis, the merit of advanced engines is measured by the improvement of the ultimate product, that justifys the introduction of new-technologies. The effectiveness of the engine mission can be improved by an increase of components efficiency level and a better integration of technologies that are interrelated in the design activities, the development tests and the manifacturing processes.

From a recent study on small turboshaft/turboprop engine in the nominal 850 shp size [1], considering advanced, simple and recuperative cicle technology (production in 1990's) and far term regenerative cicle (production post 2000), the authors reach the conclusion that the reduction of Specific Fuel Consumption (SFC) can be between 21-37% and of Life Cycle Cost (LCC) can be between 24-38%, using advanced tech, while these values are 50% for SFC and 38% for LCC respect to the actual level, with the far term tech. Key-technology areas are advanced wide-range axial-centrifugal compressor, advanced single stage high pressure turbine and ceramic composite materials.

1.2 Benefit of increasing turbine performance

The importance of the contribution of the turbine component in the improvement of the engine performances (with TET in the range 1480-1645 kelvin, and cicle pressure ratio 12-14), is due to the fact that the target increase of efficiency is expected to be from one up to four more points, respect to the actual level. This goal will be performed in conjunction with the reduction of the weight and of the cooling flows, through the application of different technologies, like advanced aerodesign methods, composite ceramic static parts and casting cooling passages.

1.3 Axial turbine stage evolution

The core engine turbine of such class of turboprop-shaft below 1500 shp has a number of design constrains due to manifacturing cost and component life, as pointed out recently by Okapuu [2], regarding the static and rotating blade trailing edge high blockage, high tip clearance (up to 3% of blade span) and low blade aspect ratio (down to 0.3 for NGV). So that the losses due to secondary flows and rotor tip clearance are more important respect to an equivalent configuration in larger engine. This is the main reason of the actual reduced performances of the "small" turbines, tacking into account also that the cooling benefits of the rotor blade can be offset by penalty in aerodynamic and additional losses.

The requirement of reducing the initial cost of the engine strongly suggests the reduction of the number of the stages, and so the gas-generator turbine for this class of engines will be not only "small" but also "high loaded", that means high stage loading and high expansion ratio. This is the actual tendency of advanced axial turbine stage, that must be efficiently air-cooled under operating transonic flow conditions.

Before looking briefly at the behaviour of such flowfield, we remark the necessity of an integrated advanced aero/mechanical performance approach, as stated by Hormouziadis and Albrecht [3], to design such turbine stage. This is important, since the aerodynamic performances are related with the cooling flows, but there is also an interaction between the incoming non uniform temperature gas-path, the secondary flows evolution and the presence of film cooling on the blade and the platforms, that has a strong influence on metal temperature distribution.

Some recent literature about research programs on high loaded axial turbine stage [4], [5], confirm that design point efficiency level of 82-87% can be reached in the single-stage axial flow turbine class of 2.1-2.5 loading factor, 3.8-4.5 expansion ratio. These results can be still improved by the incorporation of advanced computational fluid dynamics tools in the design procedure.

1.4 ARA research program on high performance axial turbine stage

A research program on advanced performance high temperature axial turbine stage is in progress at ALFA ROMEO AVIO since 1985, and the aim is to develop the modern design technology for this class of turbomachines, that have a significative impact on the competitiveness of the future engines. A previous experience in the field of small turboprop engine, had in mid 70's in collaboration with Rolls Royce Company, has been extended in the field of blade interactive design, advanced viscous and

inviscid CFD analysis, sofisticated cooling techniques, for the turbine aero-thermal design.

New experimental measurement techniques have been adopted on cold and hot turbine rig, designed by ARA, to understand physical phenomena and validate computational methods. The potential improvements of the know-how is progressively transferred to the design, manufacturing and test of turbine stages working at higher inlet gas temperature (1400-1800 deg K). The advantages we expect are the reduction of time and cost of the aero-thermal design, the improvement of the performances at higher inlet gas temperature and the validation of the design/calculation criteria in the field of small transonic axial turbine stage.

In the following, an overview of some significant results obtained in a typical application of a CFD 3-D analysis of a transonic gas-generator turbine stage is presented. Besides the potentiality of this tooling is shown by the comparison of numerical results with the first set of measurement, obtained at the exit plane of the NGV blade row in a full size cold-air-turbine rig at design condition, using a laser anemometry technique.

2. THE AERODESIGN OF ADVANCED TRANSONIC AXIAL TURBINE STAGE

2.1 Complex 3-D flow in the stage and numerical solving approaches

The difficulties in handling the transonic flowfield of such turbine stage are mainly due its 3-D structure. The contribution of different factors leads to this complexity. Radial distribution of blade aerodynamic loading produces strong pressure gradients inside the annular blade rows. The shock wave system is typically 3-D, due to the variation of exit Mach number along the span of the blade rows.

Besides, it is well known the inviscid flow phenomena due to the incoming radial non uniform flow subject to a deviation through a linear turbine cascade, that consists in a redistribution of vorticity with the formation of the "horseshoe vortex" and "passage vortex" [6].

The viscous effects inside the blade row produce the development of 3-D boundary layers flow along the hub and tip platform on the annulus. Last but not least, there is a strong interaction between static and rotating blade rows, that is responsible of the unsteady flow conditions.

Different CFD approaches are in use, and under development, to analyze this type of flowfield. The "state-of-art" technology is oriented in two directions : the fully 3-D steady compressible Navier-Stokes solver for turbine annular blade rows [7], and the fully 3-D unsteady compressible Euler solver for turbine stage. [8]. These numerical approaches, still under development, require the new generation machines to be included in the design procedure, since they need large-memory faster computer.

The actual trend is to do extensive application of a 3-D steady inviscid flow analysis of the turbine blade rows and stages, by Euler solvers, trying to incorporate this CFD technique efficiently in a turbine design procedure.

2.2 Experimental support for CFD development

In any case, to validate CFD codes, it is fundamental to have available good database of experimental detailed measurements of such flowfield, 3-D transonic, and this is a very hard target to reach. Starting from the incompressible flow, good results have been obtained by detail measurements with the classical instrumentation for linear cascade [9] inside the NGV and rotor type of blade rows. Successively, this type of investigation has been extended to annular NGV blade row [10] , [11] in order to understand the main flow mechanism of secondary flows in a configuration similar to the real turbomachine. Typical work in this area is the assessment of semi-empirical formulations to predict losses and flow deviation at the exit of the blade row [12], [13]. Recently more attention has been given to the phenomena of 3-D wake mixing [14].

For transonic blade row it is necessary to apply non-intrusive measurement techniques and good results have been obtained in turbomachinery, using the new-technology based on laser anemometry system [15], [16].

2.3 Key-role of inviscid CFD in the design procedure

As stated before, the critical needs of the designer is the accurate knowledge of the physical and aerothermal process as influenced by flowpath hardware. Following the classification recently done by Simoneau and Hudson [17], about the use of CFD in (1) routine design, (2) developmental "problem solving" or "design cecking", and (3) detailed analysis, the 3-D inviscid CFD by Euler codes is a specific tool of the second level, applied in the design process after the first one (2D inviscid, boundary layer codes), and before the third one (3-D Navier-Stokes codes).

In fact in this phase of the design procedure the analysis of the 3-D transonic flowfield inside turbine blade rows relative to the steady inviscid situation is performed to refine the geometry. The method is based on the solution of the fully 3-D Euler equations applied to the blade row computational domain, without doing any distinction between primary and secondary flows.

This analysis can be done at two different levels. In a preliminary phase, the solution of 3-D transonic flowfield in the blade row can be obtained with a conservative code using a coarse mesh, so that the turbine aerodesigner can evaluate blade loading, 3-D shock structure, main flow deviation and identify critical flow areas.

The other potentiality of this methodology is the capability of predicting the convection of the inlet vorticity inside the flowfield, in order to study the secondary flow behaviour and so identify the way to design innovative blade rows, aiming at reducing or incorporating these effects. Some studies seem to confirm this hypothesis [18], [19].

The Euler solvers, developed in the last decade [20]-[22], are based on different numerical schemes like finite difference, finite elements, finite volumes, to discretize the system of equations for 3-D compressible, inviscid, rotational flow.

2.4 The 3-D blade row aerodesign

The new flowfield analysis tool is successfully used in the so-called 3-D blade design method. As pointed out by different turbine designer [23], [24] the goal remains the same of the classical 2-D approach, that is a good airfoil-endwall pressure distribution, optimizing the velocity distribution and controlling the deceleration. The new-capability of the flowfield 3-D analysis allows to play not only with the profile geometry parameters, like the curvature and the thickness distribution, but also the endwall curvature of the annulus and profile blade radial staking. In this way, by controlling the radial loading, the secondary flows and also the downstream effect of secondary flows, more efficient blade rows can be designed. There are some good exemples in open literature about the application of such codes to the analysis of existing transonic turbine NGV [25] and stage blade rows [26].

Nevertheless some discrepancy about the capability of solving complex fully 3-D flow in the transonic turbine stage have been reported by Br y in a recent AGARD Conference [27], and the question of the usefulness of the application of this method to the flowfield inside the rotor blade row, with the inlet condition obtained by the simultaneus solution of the NGV blade, is still an open question.

This is one of the motivation that strongly suggest to investigate on the capability of this CFD tool in the field of transonic stage aeroanalysis, in order to explore its capability and limitations.

3. INVISCID FLOWFIELD 3-D ANALYSIS

3.1 The Euler solver

The set of programs currently used at ARA R&D are based on the work of Prof. Arts of Von Karman Institute [28]. So that we just describe the basic principle of the method, and refer for the details of the numerical method to published papers [29], [19]. The equations of motion, in cylindrical coordinates (r,θ, z), applied to the flow in an axial turbine blade row (fig.1), are written in the following quasi-conservative form :

$$\frac{\partial \vec{\sigma}}{\partial t} + \frac{1}{r}\frac{\partial}{\partial r}\left(r\vec{f}(\vec{\sigma})\right) + \frac{1}{r}\frac{\partial}{\partial \theta}\left(\vec{g}(\vec{\sigma})\right) + \frac{\partial}{\partial z}\left(\vec{h}(\vec{\sigma})\right) + \vec{b}(\vec{\sigma}) = 0$$

$$\vec{\sigma} = \begin{bmatrix} \rho \\ \rho V_r \\ \rho V_\theta \\ \rho V_z \\ \rho e \end{bmatrix} \qquad \vec{b}(\vec{\sigma}) = \begin{bmatrix} 0 \\ -\frac{1}{r}\rho V_\theta^2 - \frac{p}{r} - \rho r\Omega^2 - 2\rho\Omega V_\theta \\ \rho V_r V_\theta / r + 2\rho\Omega V_r \\ 0 \\ 0 \end{bmatrix}$$

$$\vec{f}(\vec{\sigma}) = \begin{bmatrix} \rho V_r \\ \rho V_r^2 + p \\ \rho V_r V_\theta \\ \rho V_r V_z \\ \rho V_r (e + \frac{p}{\rho}) \end{bmatrix} \qquad \vec{g}(\vec{\sigma}) = \begin{bmatrix} \rho V_\theta \\ \rho V_r V_\theta \\ \rho V_\theta^2 + p \\ \rho V_\theta V_z \\ \rho V_\theta (e + \frac{p}{\rho}) \end{bmatrix} \qquad \vec{h}(\vec{\sigma}) = \begin{bmatrix} \rho V_z \\ \rho V_r V_z \\ \rho V_\theta V_z \\ \rho V_z^2 + p \\ \rho V_z (e + \frac{p}{\rho}) \end{bmatrix}$$

where: ρ is density, p pressure, V velocity, e energy and Ω angular speed.

The closure relation is provided by the perfect gas law :

$$p = (\kappa-1)\left[\rho e - \frac{1}{2}\rho\,(V_r^2 +$$

These equations are solved by a time marching technique combined with the finite volume discretization approach, using the so-called corrected viscosity scheme. The computational grid is represented in fig. 2. It is made by up one blade passage and extends upstream and downstream. The flow domain is discretized in three kind of surfaces : the "streamwise", the "bladewise" and the "spanwise". A denser grid is used where more detailed information are desiderable.

3.2 The transonic axial turbine stage

3.2.1 Design point conditions

The stage object of this study is the first of a two-stage axial turbine of a small turboprop engine of 600 SHP. The design point conditions are presented in table T-1:

Table T-1

Turbine Stage Design Point			
		"hot"	"cold"
mass flow	kg/s	2.67	2.29
inlet temperature	deg k	1293	415
inlet pressure	kPa	640	315
pressure ratio, t-s	-	3.5	3.5
rotational speed	RPM	38100	21600

3.2.2 Blade geometry

The stator blade is fabricated from two specified blade profiles at hub and tip radius, radially staked at trailing edge. There are four slots radially equispaced at the pressure side near the trailing edge (fig. 3) for the air-cooling of the NGV blade. The exit blade angle is 71.4 deg. The rotor blade is defined by three profiles at hub, mid and tip radius with a radial stacking around a center of gravity. The rotor blade is uncooled.

The aspect ratio of the vanes and blades are respectively 0.54 and 0.8, the hub/tip ratio is 0.82, and the inter-row spacing is 30% of the blade height. The stage has 23 vanes and 39 blades.

3.2.3 Experimental overall performances

A schematic cross section of the cold-air turbine rig (fig. 4) shows the measuring stations: 1 inlet of the stage, 2 between NGV and rotor, 3 outlet of rotor.

Fig. 5 shows the performances of the stage at design speed, in terms of capacity and work coefficient vs t-s turbine expansion ratio. These results have obtained with engine hardware, but no cooling flow through NGV blade slots. The build tip clearance ratio is 1.2%. At the time of the investigation no information about turbine inlet turbulence level and

NGV inlet endwall boundary layers were available.

3.3 CFD results

The results that we are presenting are relative to two different effects on the NGV flowfield :

* inlet vorticity, due to incoming Boundary Layer at endwalls
* downstream rotor interaction, due to matching between blade rows

In table T-2 we summarize the conditions of the four calculations we have performed.

Table T-2

Test case number	blade row	inlet duct	inlet pressure gradient
1	NGV	radial	no
2	NGV	radial	yes
3	NGV	axial	yes
4	NGV+ROT	radial	no

For a greater clarity in the presentation of the results, they will be given for each numerical test, in terms of meridional flowfield. Later we will do a comparative analysis.

3.3.1 Test no. 1 : NGV with radial inlet, uniform inflow

The first calculation has been done simulating the true geometry of the annulus of the inlet duct of the turbine stage like the rig hardware. The numerical results presented here are relative to a computational grid 81x21x21, i.e. 81 spanwise, 21 streamwise and 21 bladewise surfaces, the last two equally spaced (fig. 6). The computational mesh has been extended in the streamwise upstream the leading edge of the blade to simulate correctly the inlet flow, that has uniform conditions in terms of total pressure, total temperature and flow angle. The overall pressure ratio was set by fixing the static pressure at the hub at the exit to the value 0.457. The convergence of the calculation was cheked using pichwise mass-average blade-to-blade flow angle , stabilized within 0.2 deg.

In fig. 7, we present the blade-to-blade Mach number distribution at mid and tip radius. Transonic flow conditions are observed at the NGV exit, where the sonic line in the throat region and supersonic pocket at suction side MID section (isentropic Mach Number 1.1) are detected. The iso-Mach contours in the meridional plane at pressure and suction surface are shown in fig. 8. Here we can observe the basic 3-D flow structure, due to different loading distribution and exit Mach number between hub and tip radius. Supersonic flow region up to Mach 1.2 are confined near the HUB at Blade suction side (SS).

3.3.2 Test no. 2 : NGV with radial inlet, inlet vorticity

The aim of the second calculation is to visualize the effect of inlet vorticity on the NGV flowfield, due to boundary layer (BL) development on the sidewalls of the inlet duct. The computational mesh has been streched enough, increasing the number of streamwise surfaces (81*21*41) (fig. 9). Our intention is to simulate the BL , and so we estimate the 2-D BL parameters at hub and shroud based on the velocity distribution of test case no. 1, and than the relative non uniform total pressure variation normal to the walls (fig. 10-a) has been imposed to the first stanwise station as inlet boundary condition. For exit boudary condition the static pressure at the hub was fixed to 0.457.

The results of the calculation in terms of iso-Mach contours in meridional plane are shown in fig. 11, on pressure and suction surfaces. Respect to the previous numerical test case, where no vorticity is imposed to the inlet flow, we do not observe any significative difference in the Mach number distribution near the blade surfaces. Let's note that the total pressure radial profile near the hub and tip endwalls, in proximity of the LE station, are smoother than the one imposed at the inlet station (fig. 10-b). So, we try to reduce this undesiderable effect, that we suppose is due to numerical dissipation, in the following calculation, modifying the mesh topology.

3.3.3 Test no. 3 NGV with axial inlet, inlet vorticity

The computational domain has been simplified at the inlet of the NGV, using a cylindrical annulus geometry. This means that in this case we do not simulate the real fully radial inflow conditions, since we impose axial inflow, nevertheless we have applied the inlet vorticity due to BL presence on the endwalls, and we expect that the simulation is more realistic respect to the previous calculation. The computational mesh is 81x21x41 (fig. 12). Also in this case we imposed as boundary exit condition, the static pressure at the hub to the value 0.457. From the iso-Mach contours distributions, shown in fig. 13, we conclude that the difference in the flowfield respect to the previous calculation (test no. 2) is limitated to the blade L.E. region and it is due to the geometry of the inlet duct.

3.3.4 Test no. 4 : NGV+Rotor with radial inlet, uniform inflow

The last numerical test has been performed on the stage at design speed. A special version of the code can handle this calculation based on the hypotesis of time average flow. Upstream of each blade row, along the span, the tangential variation of all flow properties is set to zero, providing a mean or steady interaction between fixed and rotating blade rows. Two interconnected 3-D blade row calculations are performed simultaneously : one in the stator and one in the rotor. The inter-row boundary conditions are repeatedly adapted until stabilization and corrispondence of mass flow in both blade rows. The calculation has been performed on a 59x11x11 grid for each blade (fig. 14). In this case a multiple grid was used : the calculation starts fist on a coarse mesh (30x6x6) and then swiches to the final grid. As boundary conditions, upstream we set uniform flow, as test case no. 1, while at stage computational domain downstream, the static pressure at exit of the rotor at hub radius was imposed.

The iso-Mach contours plot on suction and pressure surfaces in the meridional plane are shown in fig. 15. From the comparison between the NGV flowfield obtained by stage calculation, respect to the one of the NGV "only" (test case no. 1, fig. 8), we note that the presence of the rotor influence the NGV flowfield primarly in the region behind the NGV TE, modifying the radial static pressure gradient, and, although the static pressure at the hub at the NGV exit computational domain is sligtly different (in test case no. 1 is imposed 0.457, while in test case the final result is 0.467), a significant difference has been found in the transonic region on the suction surface.

3.4 Comparative analysis of numerical results at NGV exit

Now we look at the different flowfields from the point of view of the NGV exit, showing the structure of the inviscid 3-D transonic flowfield by the Mach number and the flow angle distributions, at a reference spanwise station, wich axial distance from the T.E. is about 18% the axial chord.

The effect of inlet vorticity on NGV flowfield, simulated in a radial inlet, is very well resolved, comparing the results from test case no. 1 and 2. In fact the secondary flows generated by the incoming vorticity, although do not modify the Mach number distribution (see figg. 16-a, 16-b), have a significative impact on the iso-Betas distribution (see figg. 17-a, 17-b), since regions of overturning appear near the endwalls.

The sensitivity of NGV flow field to inlet vorticity becomes evident from the comparison of the results of the test no. 2 and 3. In this case the effective true vorticity at the L.E. plane is greater for the test case n. 3 and so, while from fig. 16-b, 16-c, the iso-Machs change a little near the endwalls, the iso-Betas of fig 17-c respect to fig. 17-b show enlarged region of overturning, and local zones of underturning.

Finally the effect of downstream rotor row on NGV flowfield, at uniform incoming radial flow, is shown from the comparison of the results of test no. 4 respect to no. 1. Here fig. 16-d shows a lower Mach number level respect to 16-a, and the flowfield seams to be more uniform, although this may be due to the coarser mesh we used in stage calculation for spanwise surfaces (11x11) vs NGV "only" test (21x21), so that we can loose flow details. What is important to note is the significant difference observed in flow angle Beta plots, because the values of fig. 17-d are lower respect to fig. 17-a, so that the rotor interaction seams to reduce the NGV flow deviation respect to the NGV "only" flow situation, in particular way in the hub region.

4. COMPARISON WITH AVAILABLE EXPERIMENTAL DATA

An experimental investigation has been carried out on the flowfield of this transonic stage, using the well-known non-intrusive technique of laser anemometry on the cold-air turbine rig. In the ARA turbomachinery lab the Laser-Two Focus is recently available.

The application of this system to a two-dimensional mapping in turbomachinery flow situation in transonic speed range, has many advantages, like non-intrusive measuring method, backscattering, large velocity range, precise measurement of absolute velocity and flow angle, high spatial and angular resolution.

4.1 Measurement technique : laser two-focus anemometry

The Laser 2 Focus Velocimeter operates by detecting scattered lights from small particles, which are always present in the fluid, as they pass through two focal volumes formed by laser beams (fig. 18). The velocity is derived from the time of flight of particles moving from one beam waist to the other and the known separation of the two beam waists. This technique is sometimes called Laser Transit Anemometry. For more details about this system delevoped at DFVLR see ref. [30]. The system we have used is made by POLITEC, and consists of the optical heads (optical elements, photodetectors, mechanical and electrical parts and a laser) (fig. 19), the signal processor and the control processor.

4.2 Presentation of results at NGV exit plane

The cold-air turbine rig was modified, to introduce the optical access for the anemometry laser system. A quarz window has been designed to be applied on the casing of the rig in corrispondence to the rotor blade row, with the aim to map the flowfield from NGV exit to rotor exit plane. (fig. 20).

The measurements have been carried out on the NGV exit plane in the inter-row space at 4 mm from T.E of NGV blade. The investigation has been performed at turbine design speed, near the design expansion ratio. The flowfield has been explored by a matrix of 10x9 measuring points in tangential (blade-to-blade) and radial (hub-to-shroud) directions. The system measures the module of velocity and the flow angle respect to the direction of the turbine axis.

The first results we get, relative essentially to the core flow, are presented in terms of iso-Machs in fig. 21/a, and iso-Betas in fig. 21/b.

4.3 Comparison with predictions

It is interesting to note how the main structure of the 3-D transonic flowfield is quite well predicted by numerical test no. 1, the NGV "only" with no-vorticity imposed at the radial inlet. In fact the periodic structure observed in the real flow (fig. 21/a) is captured.

More significant are the results of the numerical simulation of inlet vorticity (test case no. 2 and 3), since the measurements show the presence of well defined overturning regions (Beta>71.4 deg) near the hub and the tip (fig. 21/b), although this first set of data are relative to the core flow. The prediction of the iso-Betas of test case no. 3 (fig. 17-c) are quite similar to the experimental map of fig. 22/b.

Finally the iso-Mach plot results of the stage calculation (test no. 4, fig.16-d) are in better agreement respect to NGV "only" test of fig. 16-a when we compare to experimental data of fig. 22-a. In fact the measured radial gradient is less than the prediction, and we think that this is due to the the rotor interaction.

5. CONCLUSION

A CFD inviscid analysis of a transonic 3-D flow inside an existing axial turbine stage of a small turboprop engine, give to the designer the possibility to understand the main aspect of the this type of flowfield.

Experimental results obtained by mapping the core flow at the NGV exit plane, where strong is the interaction between static blade row and rotating one, and so where critical flow conditions influence the performance of the turbine, confirme the complexity of the flowfield structure.

Nevertheless the CFD tool used in this numerical investigation shows good capability to predict the behaviour of the flow, in terms of Mach number and flow angle.

The objective of further investigation in the numerical as well as experimental activity is to reach a better control of such complex flowfield, taking into account secondary flow together with interactive NGV-Rotor effect, so that a better understanding of the overall phenomena can give more chances in designing new advanced turbine stage.

REFERENCES

[1] R. Hirschkron, C.J. Russo
SMALL TURBOSHAFT/TURBOPROP ENGINE TECHNOLOGY STUDY
AIAA 86-1623, 1986

[2] U. Okapuu
AERODYNAMIC DESIGN OF FIRST STAGE TURBINES FOR SMALL AERO ENGINES
VKI Lecture Series on "Small High pressure ratio turbines"
VKI LS 1987-07 p. 4 , 1987

[3] J. Hourmouziadis, G.Albrecht
AN INTEGRATED AEROMECHANICAL PERFORMANCE APPROACH TO HIGH TECHNOLOGY TURBINE DESIGN
AGARD PEP on "Advance Technology for Aero Gas Turbine Components"
AGARD-CP-421 p. 11 , 1987

[4] U. Okapuu
HIGHLIGHTS FROM A RESEARCH PROGRAM ON A VERY HIGHLY LOADED AXIAL GASGENERATOR TURBINE
VKI Lecture Series on "Small High pressure ratio turbines"
VKI LS 1987-07 p. 4, 1987

[5] I.D. Brice, M.R. Lithchfield, N.P. Leversuch
THE DESIGN PERFORMANCE AND ANALYSIS OF A HIGH WORK CAPACITY TRANSONIC TURBINE
ASME 85-GT-15 , 1985

[6] J. Moore
3D FLOWS IN TURBINE BLADE ROWS
VKI Lecture Series on "Numerical methods for flows in turbomachinery"
VKI LS 1989-06 p. 9 , 1989

[7] D. Choi, C.J. Knight
COMPUTATION OF 3-D VISCOUS ANNULAR CASCADE FLOWS
AIAA 88-3092 , 1988

[8] M.B. Giles
STATOR/ROTOR INTERACTION IN A TRANSONIC TURBINE
AIAA 88-3093 , 1988

[9] P.H. Marchal, C.H. Sieverding
SECONDARY FLOWS WITHIN TURBOMACHINERY BLADING
AGARD PEP Meating on "Secondary flows in turbomachinery",
AGARD-CP-214 p. 11, 1977

[10] C.H. Sieverding, W Van Hove, E Boletis
EXPERIMENTAL STUDY OF THE THREE-DIMENSIONAL
FLOWFIELD IN AN ANNULAR TURBINE NOZZLE GUIDEVANE
ASME 83-GT-120 , 1983

[11] A. Yamamoto, R. Yanagi
PRODUCTION AND DEVELOPMENT OF SECONDARY FLOWS AND LOSSES
WITHIN A THREE-DIMENSIONAL TURBINE STATOR CASCADE
ASME 85-GT-217 , 1985

[12] D.G. Gregory Smith, C.P. Graves, J.A. Walsh
GROWTH OF SECONDARY LOSSES AND VORTICITY IN AN AXIAL TURBINE CASCADE
ASME 87-GT-114 , 1987

[13] O.P. Scharma, T.L. Butler
PREDICTION OF ENDWALL LOSSES AND SECONDARY FLOWS
IN AXIAL FLOW TURBINE CASCADES
ASME 86-GT-228 , 1986

[14] A. Binder, R. Romey
SECONDARY FLOW EFFECTS AND MIXING OF THE WAKE
BEHIND THE TURBINE STATOR
ASME 82-GT-46 , 1982

[15] L.J. Goldmann, R. G. Seasholtz
LASER ANEMOMETER MEASUREMENTS IN AN ANNULAR CASCADE OF CORE
TURBINE VANES AND COMPARISON WITH THEORY
NASA TP-2018 , 1982

[16] H. Binder, R. Schodl, A Binder, R. Dunker
SUCCESSES IN THE APPLICATION OF LASER VELOCIMETRY
TO TURBOMACHINERY STUDIES
CONCEPTS L.S on "International *Seminar on advance*
turbomachinery perfomance" , 1985

[17] R.J. Simoneau, D.A. Hudson
CFD IN THE CONTEST OF IHPTET - THE
INTEGRATED HIGH PERFORMANCE TURBINE TECHNOLOGY PROGRAM
AIAA 89-2904, 1989

[18] D. Graham Holmes, R.E. Warren
DETAILED STUDIES OF INVISCID SECONDARY FLOWS
Paper presented at 7th ISABE , 1985

[19] T. Arts
EFFECTS OF TIP ENDWALL CONTOURING ON THE THREE DIMENSIONAL
FLOW FIELD IN AN ANNULAR TURBINE NOZZLE GUIDE VANE
PART 2 - NUMERICAL INVESTIGATION
ASME 85-GT-108, 1985

[20] J.D. Denton
THE CALCULATION OF FULLY THREE DIMENSIONAL FLOW THROUGH
ANY TYPE OF TURBOMACHINERY BLADE ROW
AGARD L.S. on "3-D Computation techniques applied to internal
flows in propulsion systems"
AGARD L.S. No. 140 , 1985

[21] C.F. Shieh, R.A. Delaney
AN ACCURATE AND EFFICIENT EULER SOLVER FOR
THREE-DYMENSIONAL TURBOMACHINERY FLOWS
ASME 86-GT-200, 1986

[22] D. Graham Holmes
INVISCID 3D SOLUTION METHODS
VKI L. S. on "Numerical methods for flows in turbomachinery"
VKI LS 1989-06 p. 1 , 1989

[23] J. Hourmouziadis, N. Hubner
3-D DESIGN OF TURBINE AIRFOILS
ASME 85-GT-188, 1985

[24] F.W. Huber and R.J. Rowey, R.R. Ni
APPLICATION OF 3-D FLOW COMPUTATIONS TO GAS TURBINE
AERODYNAMIC DESIGN
AIAA 85-1216, 1985

[25] S.H. Moustapha, R.G. Williamson
INVESTIGATION ON THE EFFECT OF TWO ENDWALL CONTOURS
ON THE PERFORMANCE OF AN ANNULAR NOZZLE CASCADE
AIAA 85-1218 , 1985

[26] R.C. Kingcombe , J.D. Brice, N.P. Leversuch
DESIGN AND TEST OF A HIGH BLADE SPEED
HIGH WORK CAPACITY TRANSONIC TURBINE
AGARD PEP Meeting on "Advanced Technology for
Aero Gas Turbine Components"
AGARD-CP-421 p. 12, 1987

[27] P.F. Bry
BLADING DESIGN FOR COOLED HIGH-PRESSURE TURBINES
AGARD PEP Meating on "Blading Design for Axial Turbomachines",
AGARD-LS-167 p. 7, 1989

[28] T. Arts
A SET OF PROGRAMS FOR THE COMPUTATION OF 3-D TRANSONIC,
INVISCID, ADIABATIC, ROTATIONAL FLOWS OF A PERFECT GAS
IN AN AXIAL TURBINE BLADE ROWS
VKI CR 1986-25 , 1986

[29] T. Arts
CALCULATION OF THREE-DYMENSIONAL, STEADY, INVISCID FLOW
IN A TRANSONIC AXIAL TURBINE STAGE
ASME 84-GT-76, 1984

[30] R. Schodl
ON THE DEVELOPMENT OF A NEW OPTICAL METHOD FOR FLOW
MEASUREMENTS IN TURBOMACHINES
Paper presented at ASME Gas Turbine Conference 1974

Fig. 1 - Blade-row Computational Domain

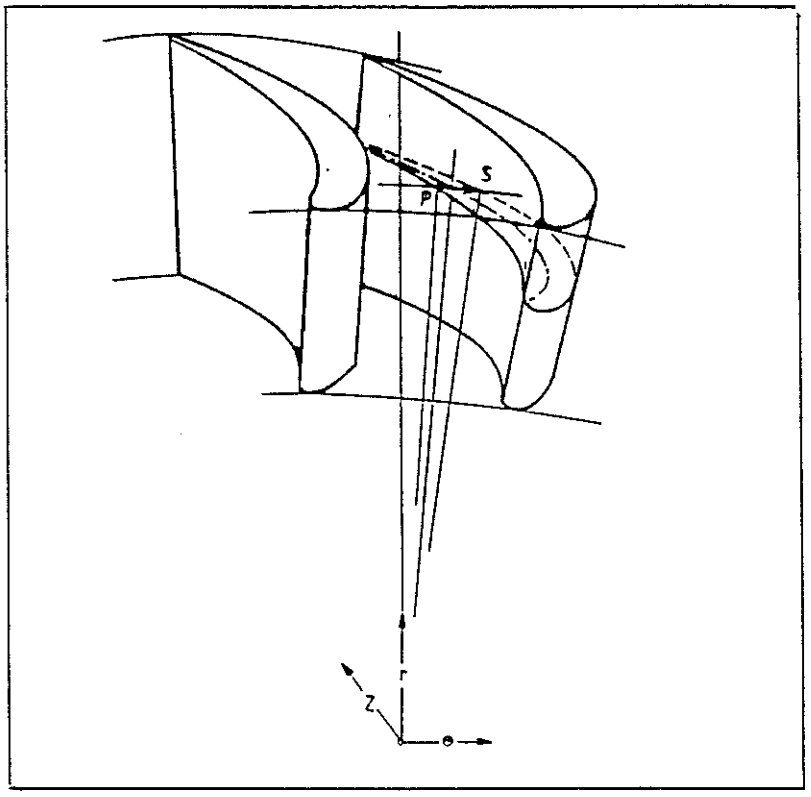

Fig. 2 - Computational grid

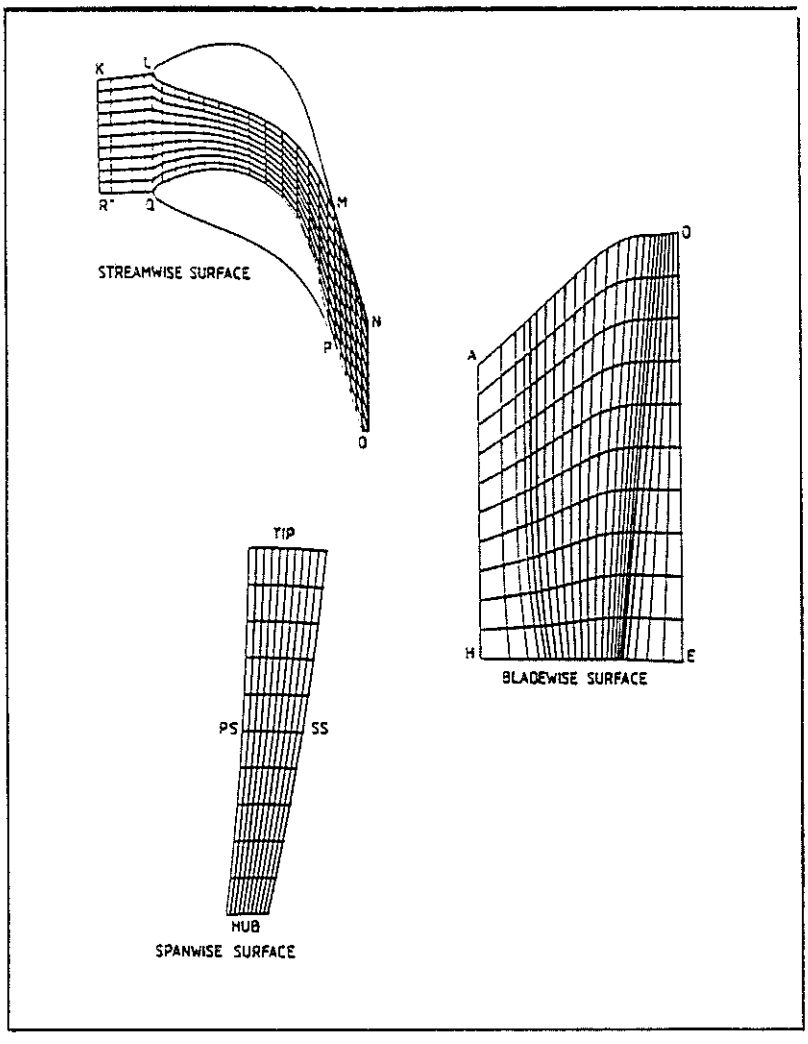

Fig. 3 - Turbine blade geometry

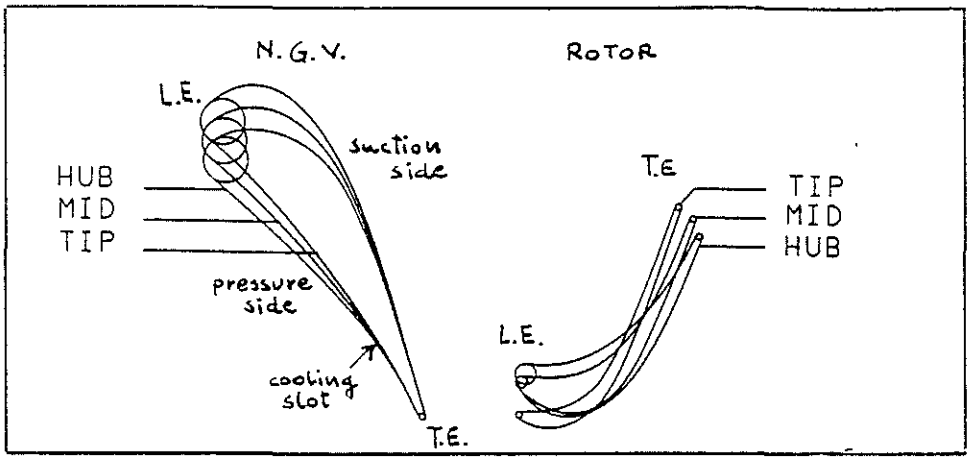

Fig. 4 - Meridional section of cold-air-turbine rig

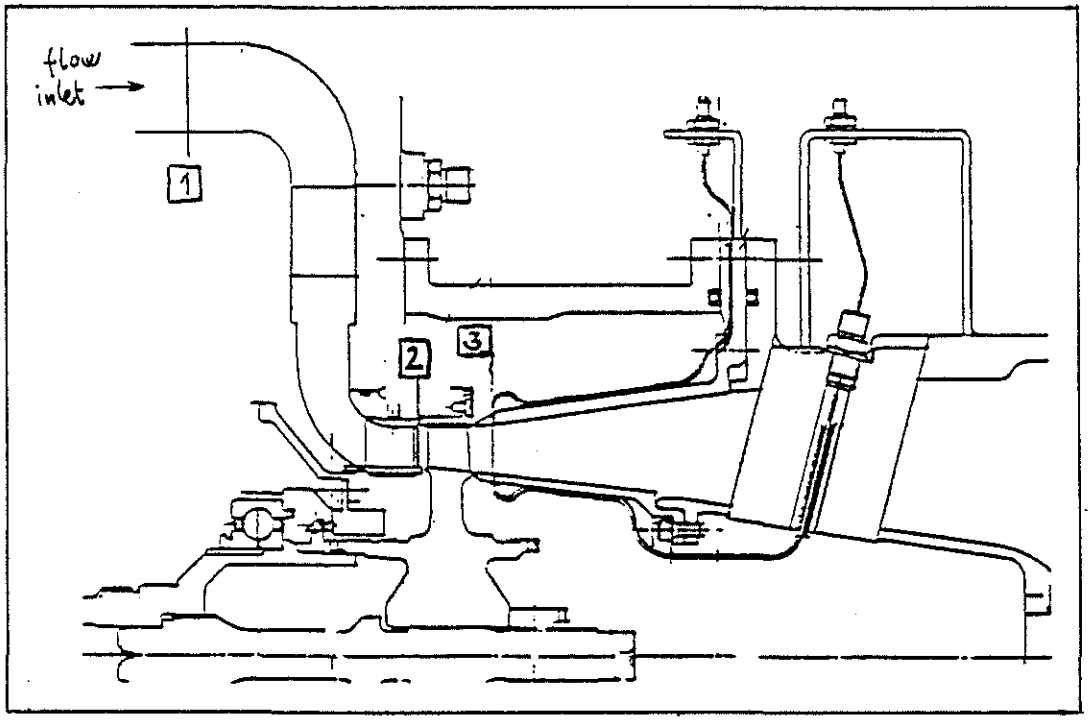

Fig. 5 - Turbine stage performances parameters vs expansion ratio, at design speed

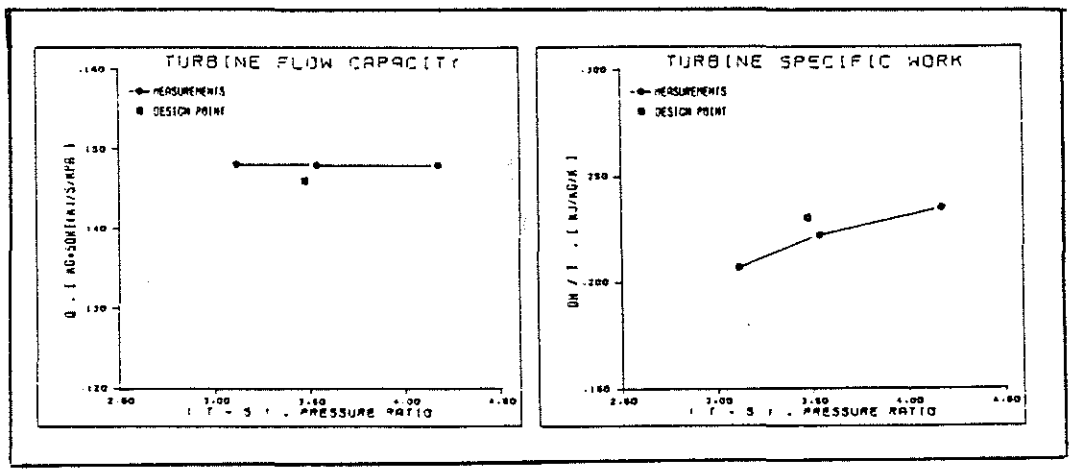

Fig. 6 - Test case 1 - Computational grid (81x21x21)

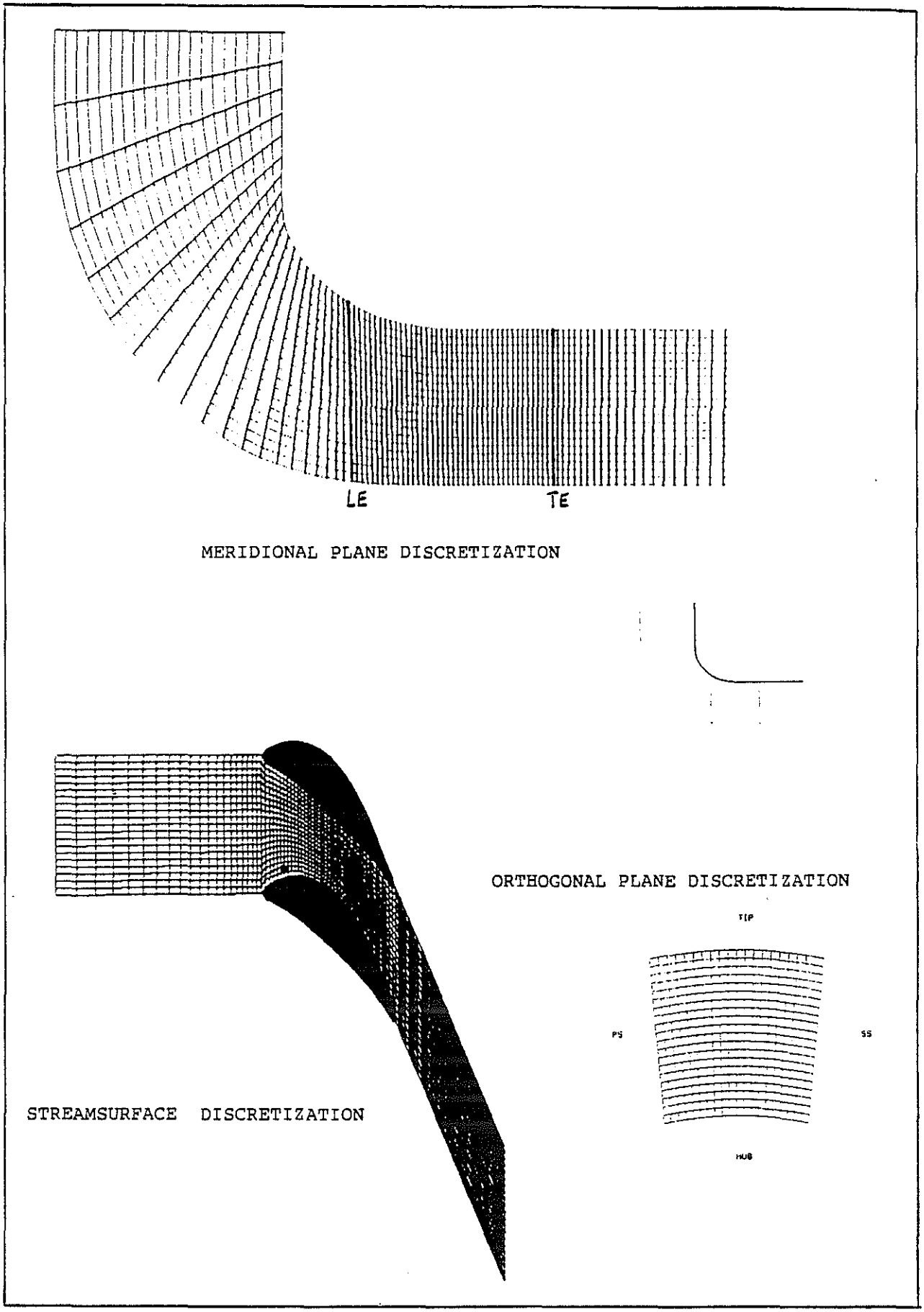

Fig. 7 - Test case 1 - Blade-to-Blade Iso-Mach contour

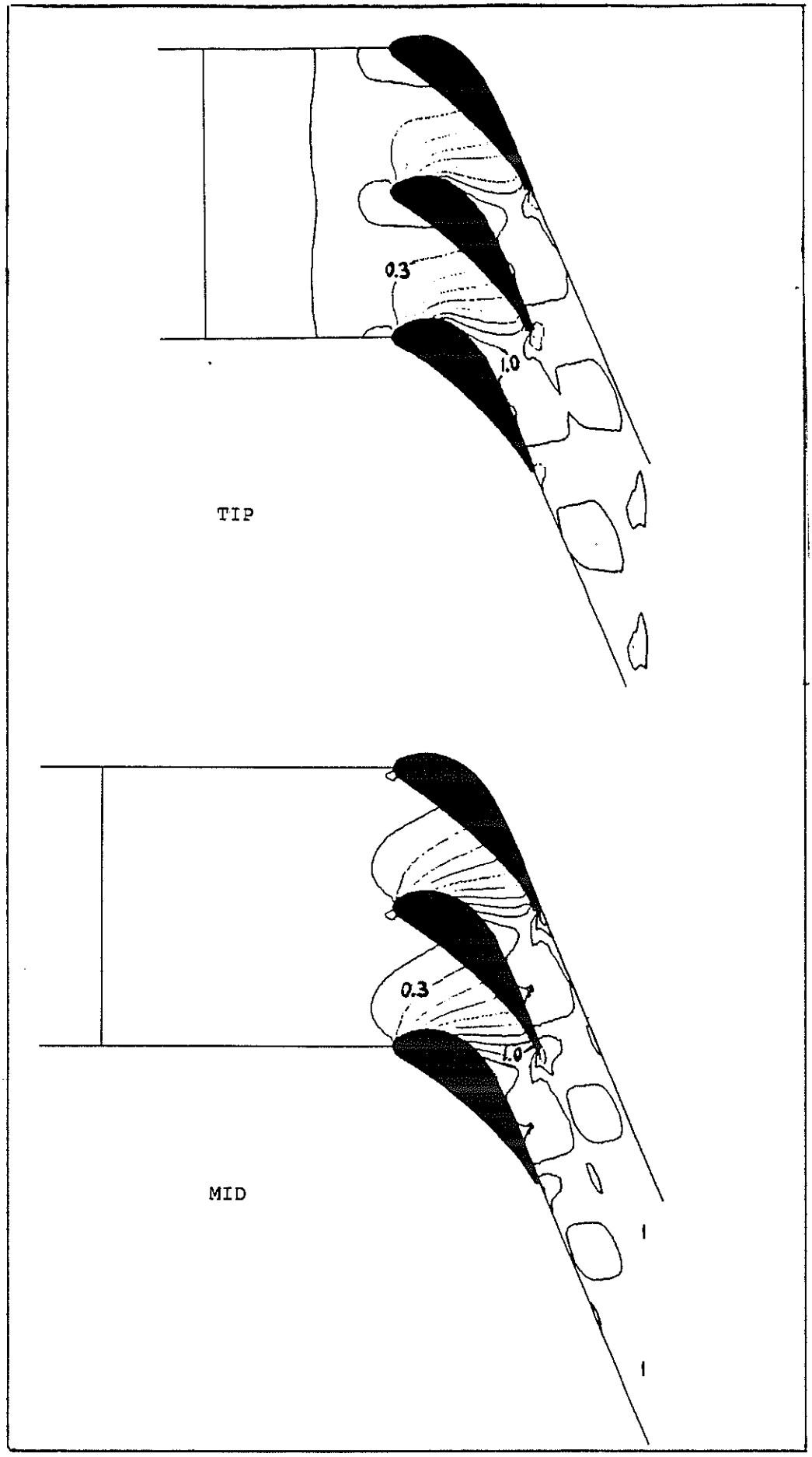

Fig. 8 - Test case 1 - Iso-Mach contour in Meridional plane

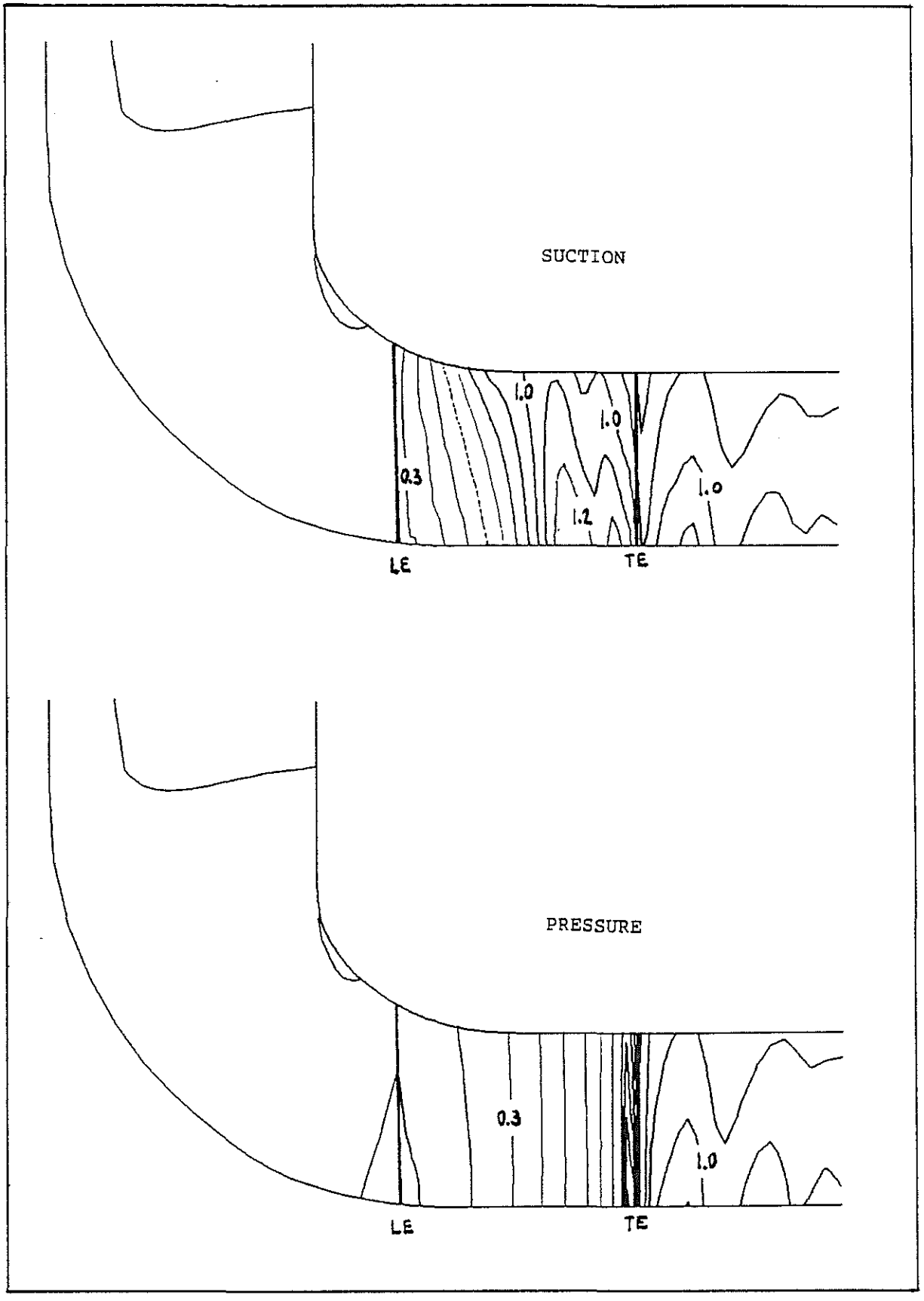

Fig. 9 - Test case 2 - Computational grid (81x21x41)

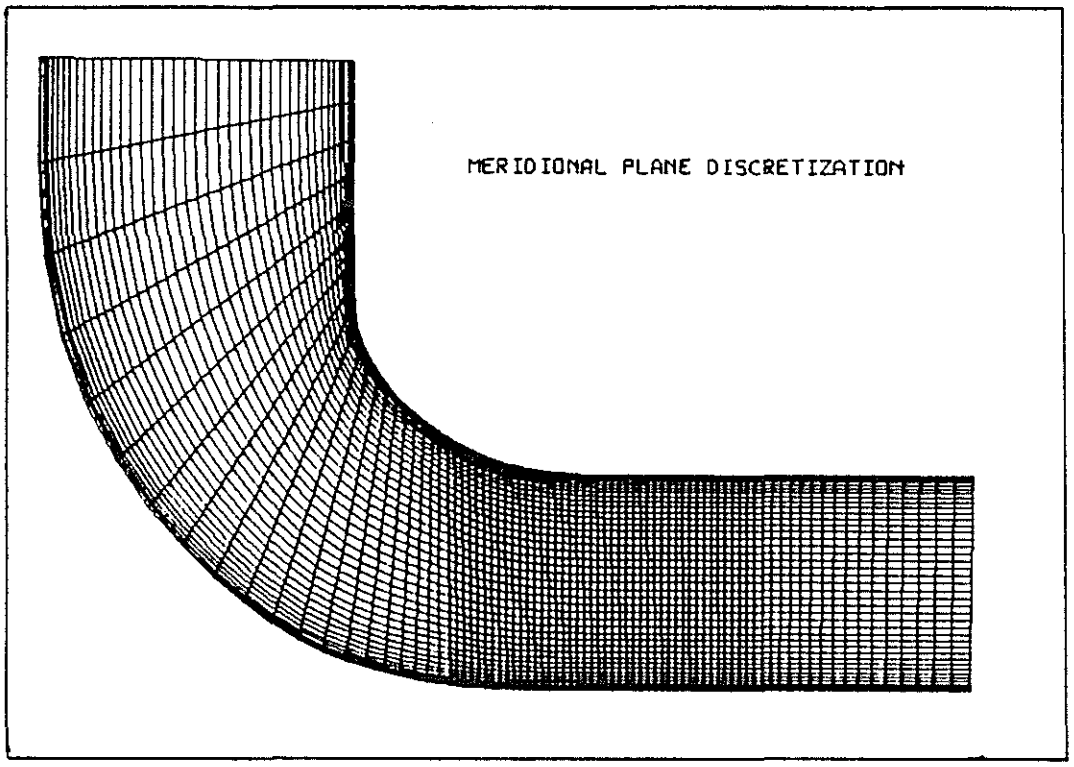

Fig.10 - Test case 2 - Non-uniform total pressure profiles

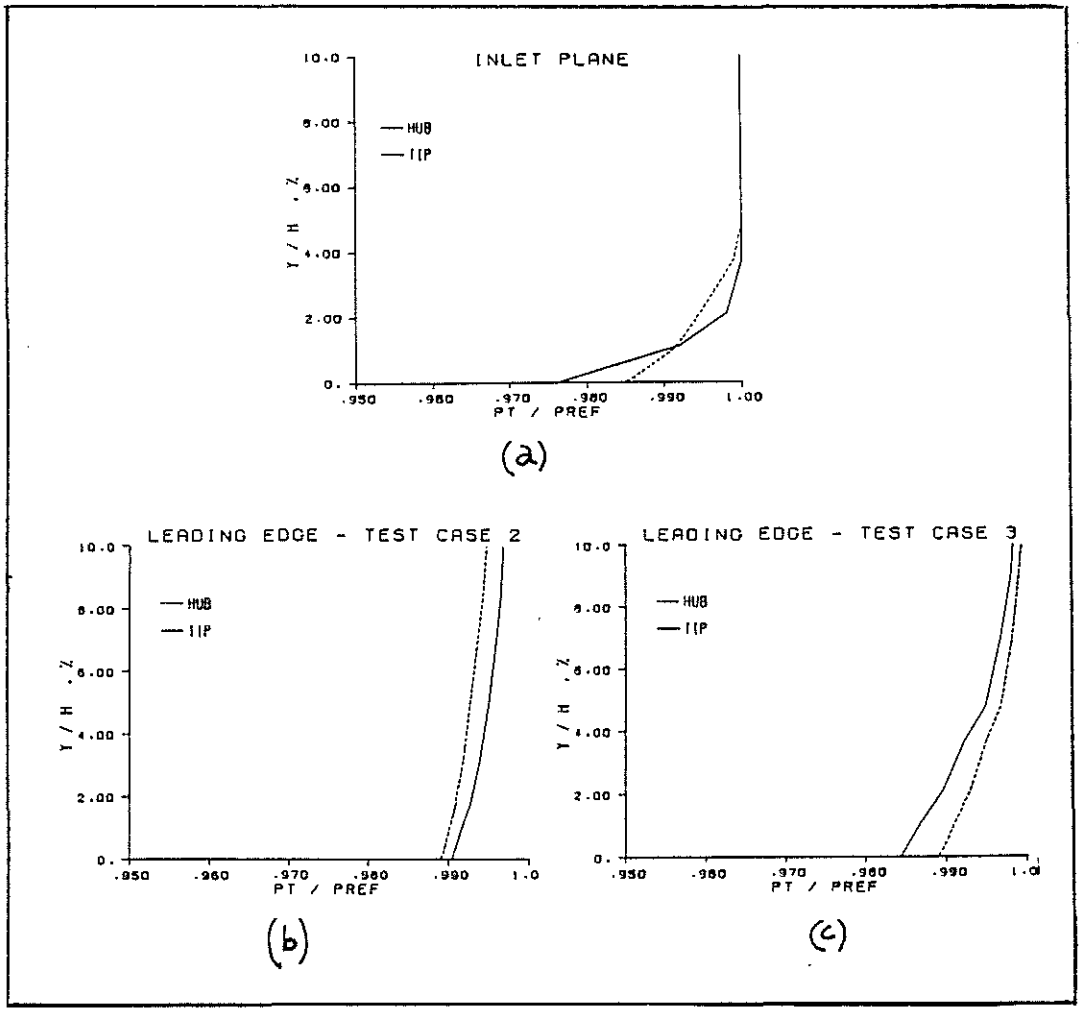

Fig.11 - Test case 2 - Iso-Mach contour in Meridional plane

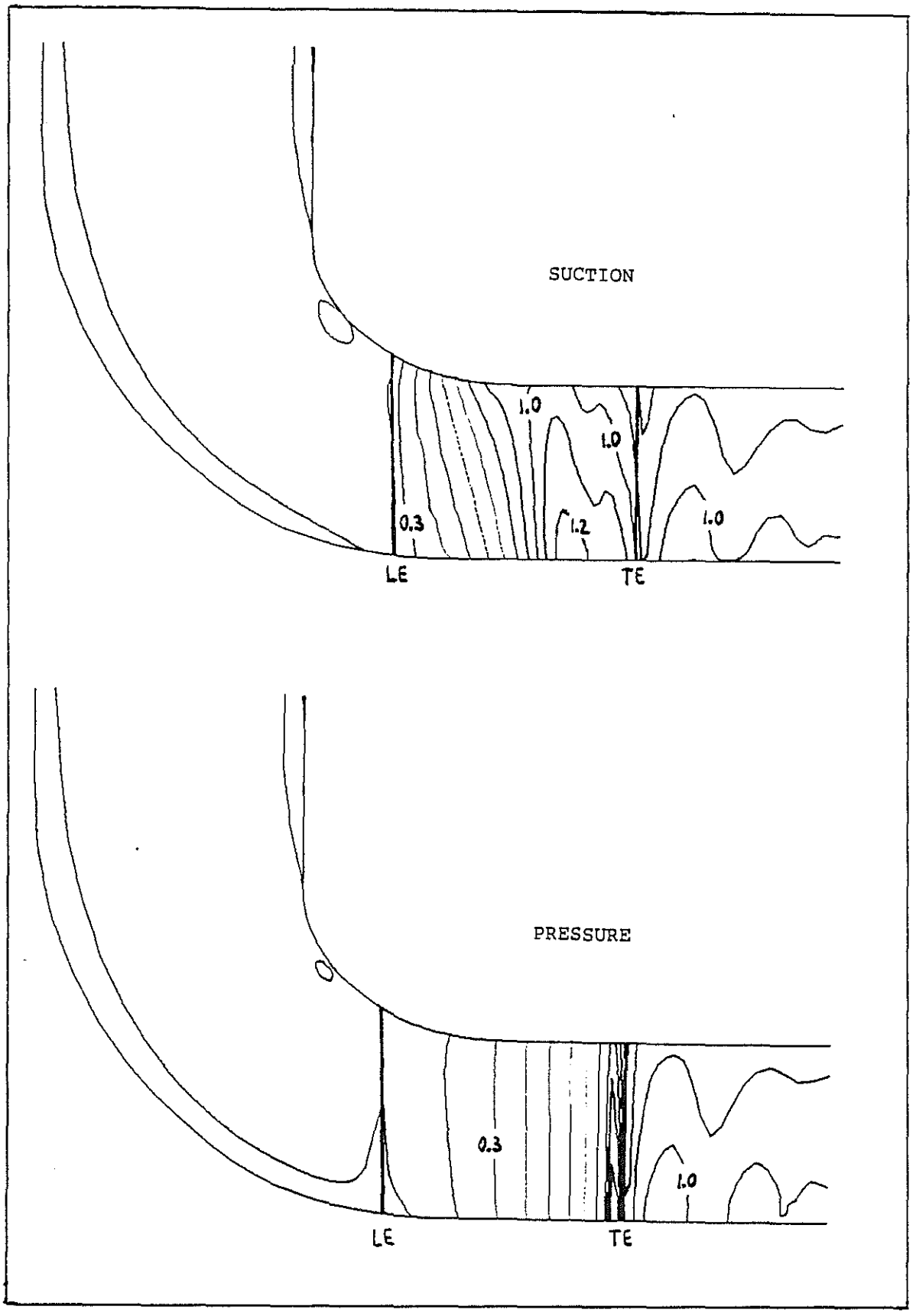

Fig.12 - Test case 3 - Computational grid (65x21x41)

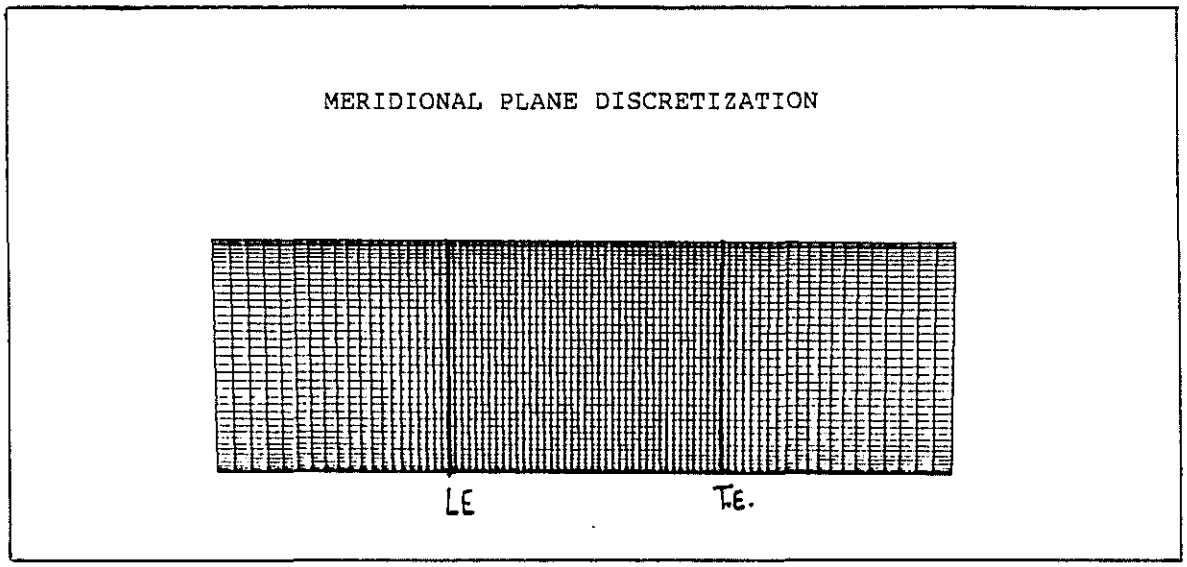

Fig.13 - Test case 3 - Iso-Mach contour in Meridional plane

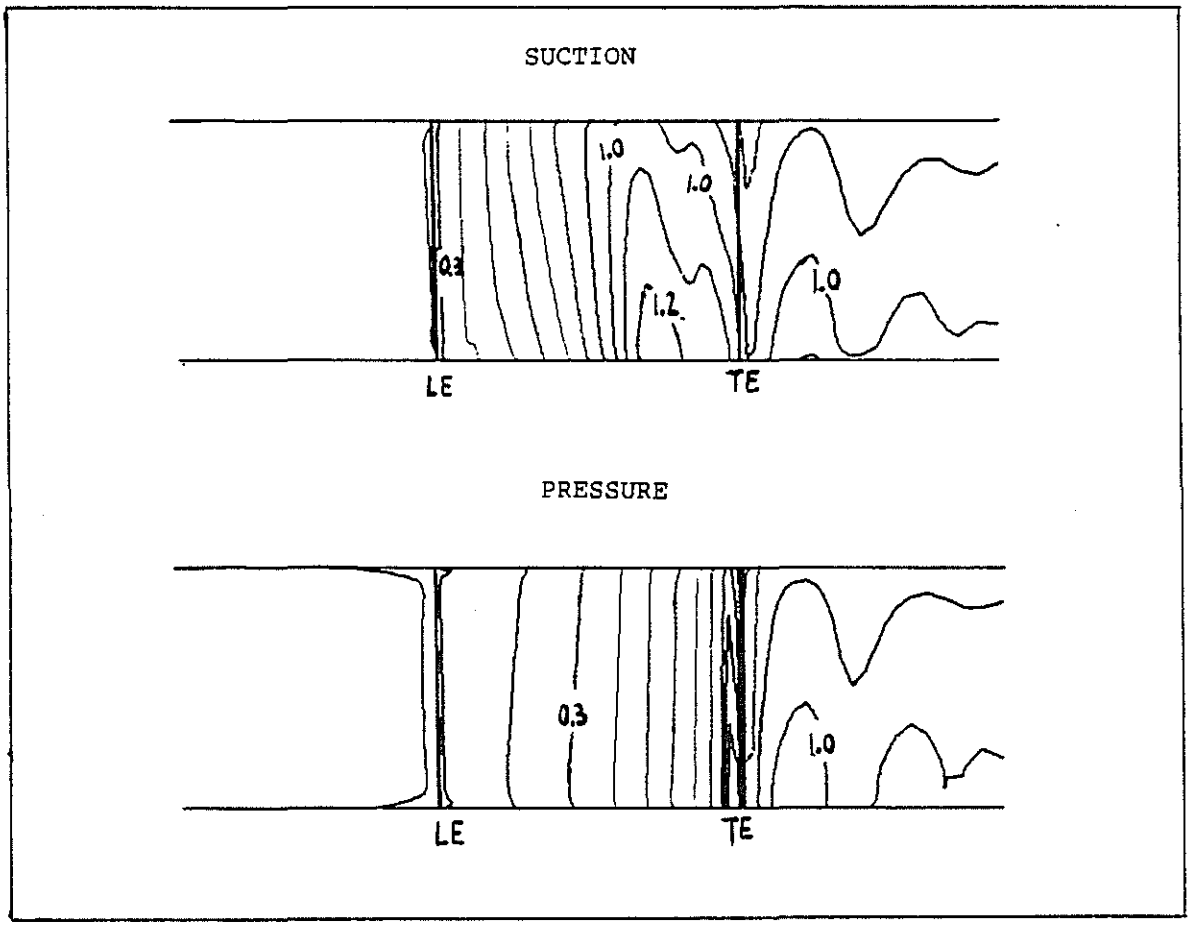

Fig.14 - Test case 4 - Computational grid (59x11x11), (59x11x11)

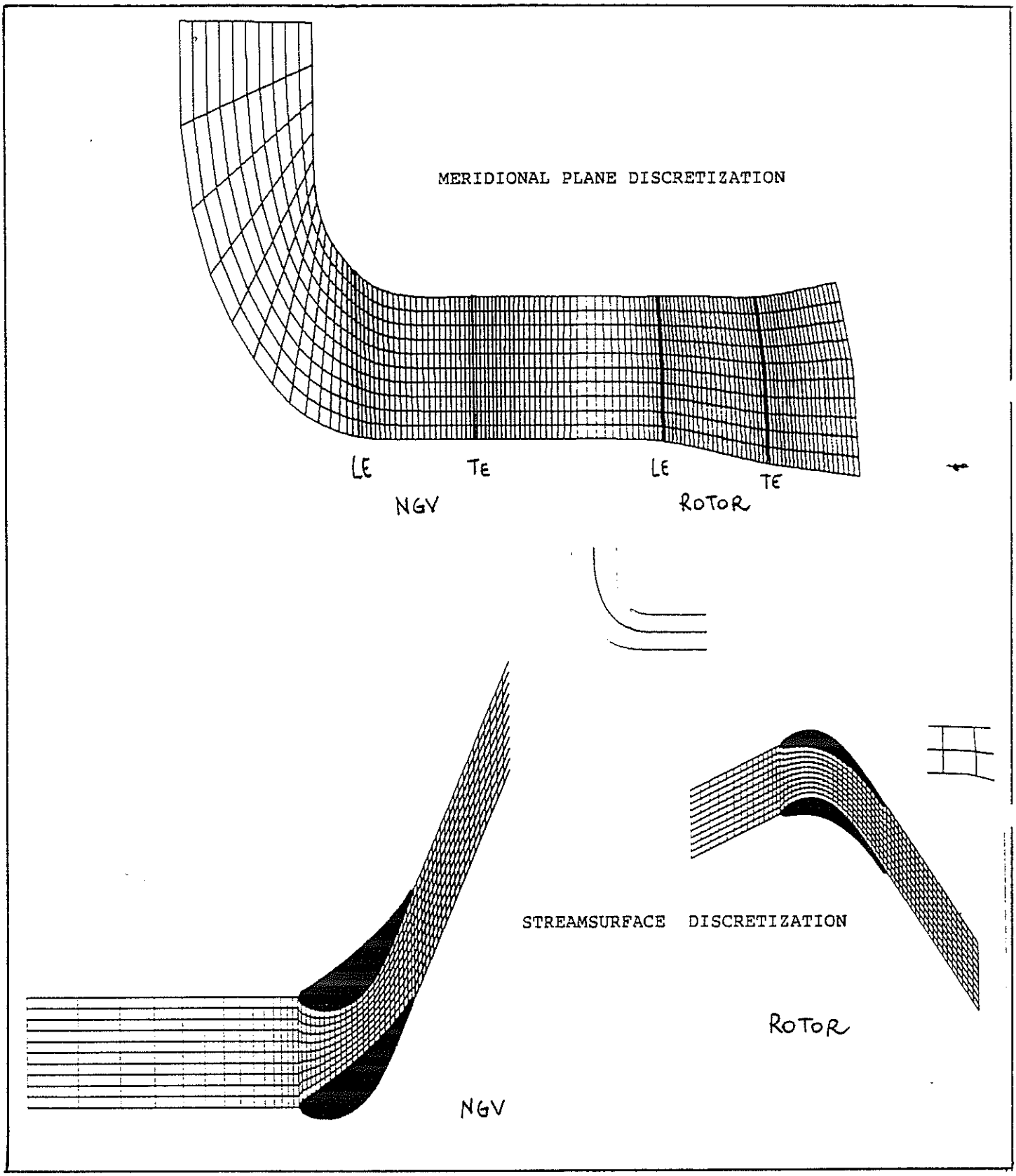

Fig.15 - Test case 4 - Iso-Mach contour in Meridional plane

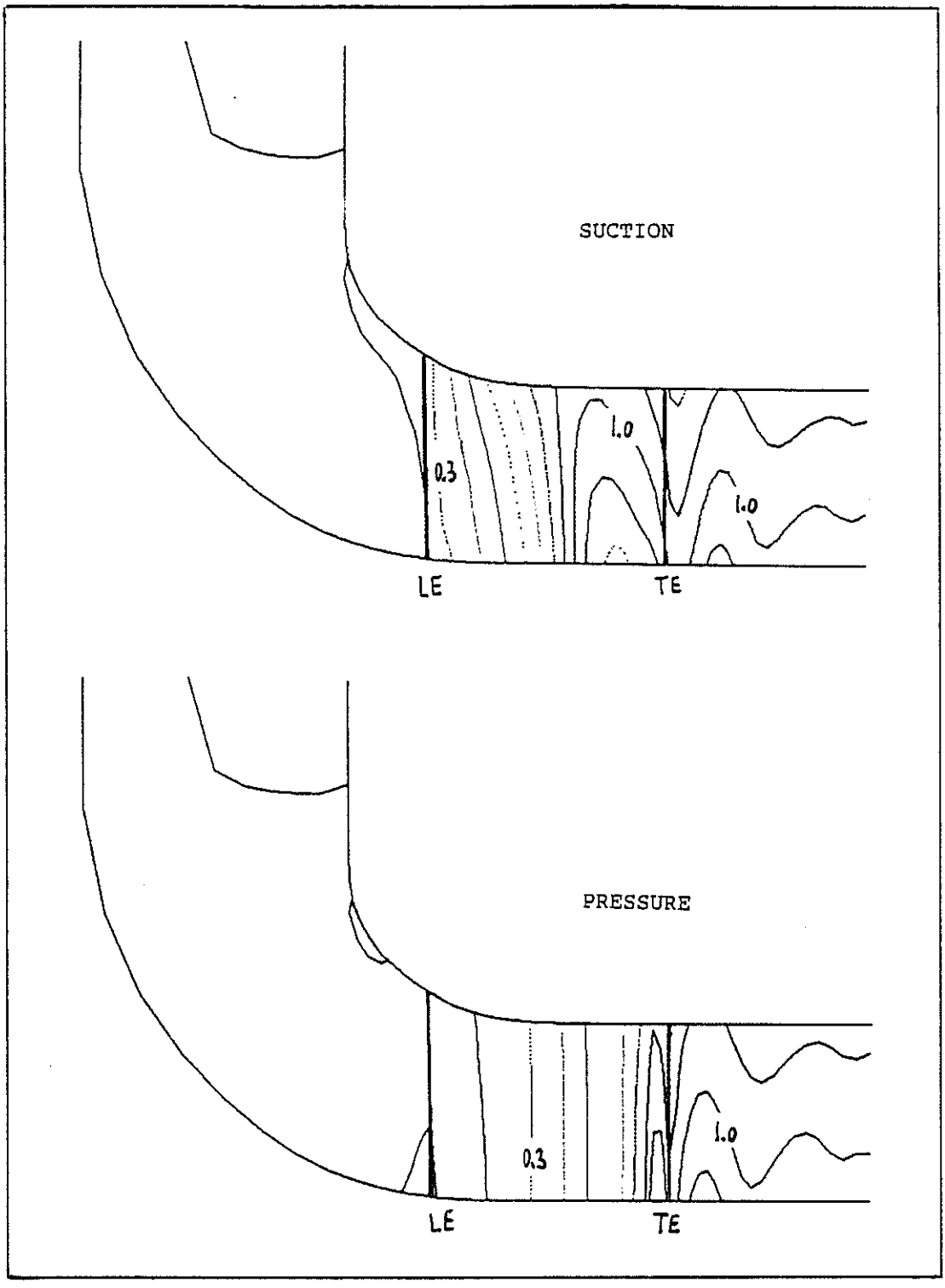

Fig.16 - Numerical test case 1,4 - NGV Exit Flow Mach Number

16-a) Test case no. 1

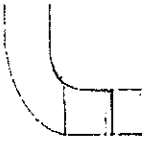

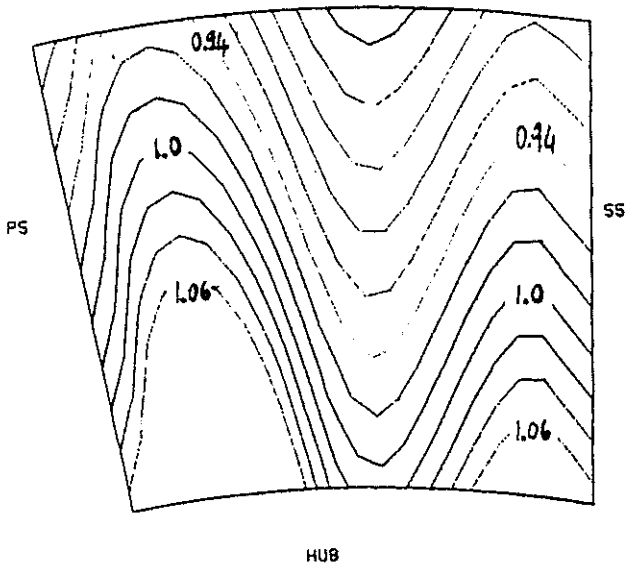

16-b) Test case no. 2

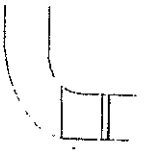

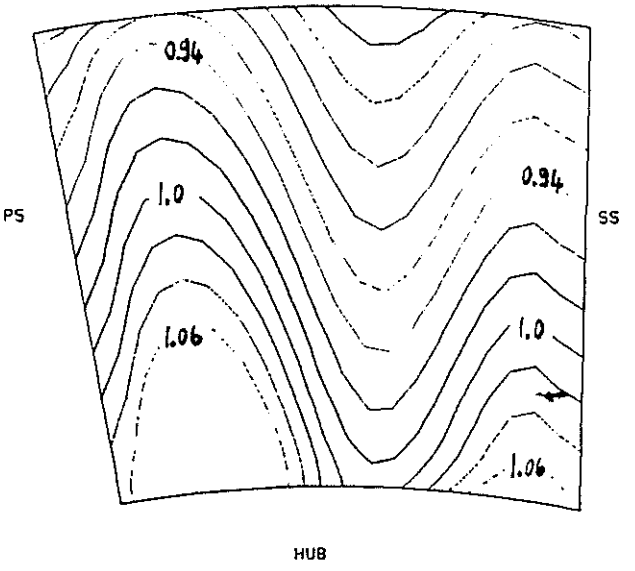

16-c) Test case no. 3

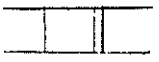

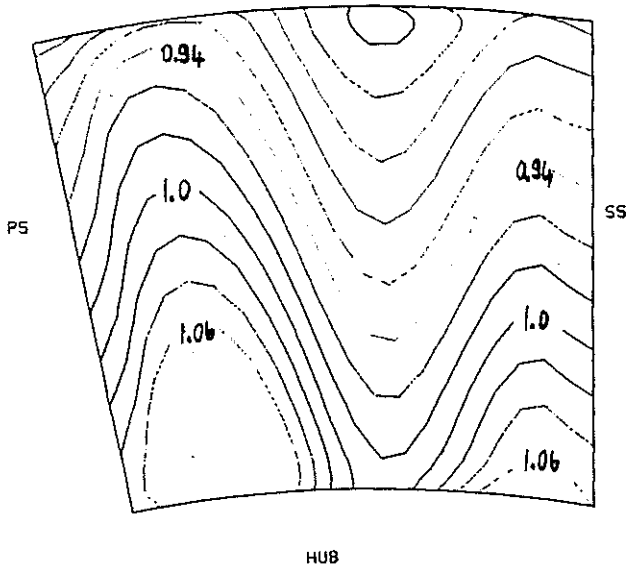

16-d) Test case no. 4

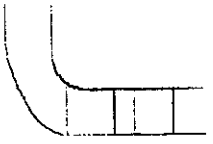

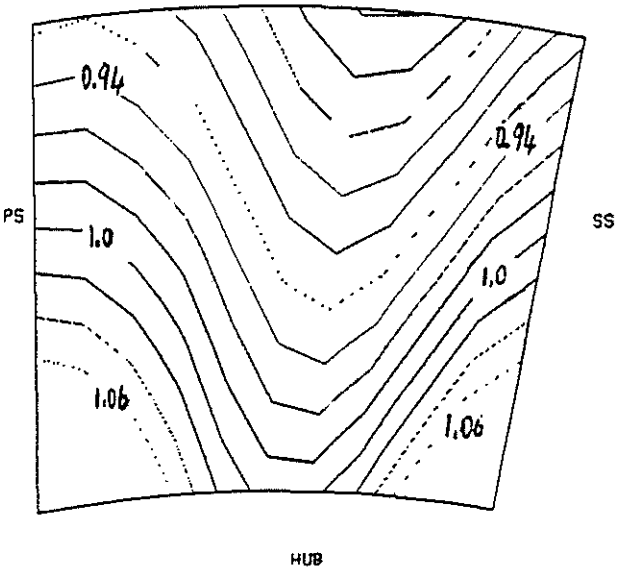

Fig.17 - Numerical test case 1,4 - NGV Exit Flow Angle Beta

17-a) Test case no. 1

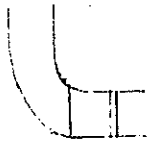

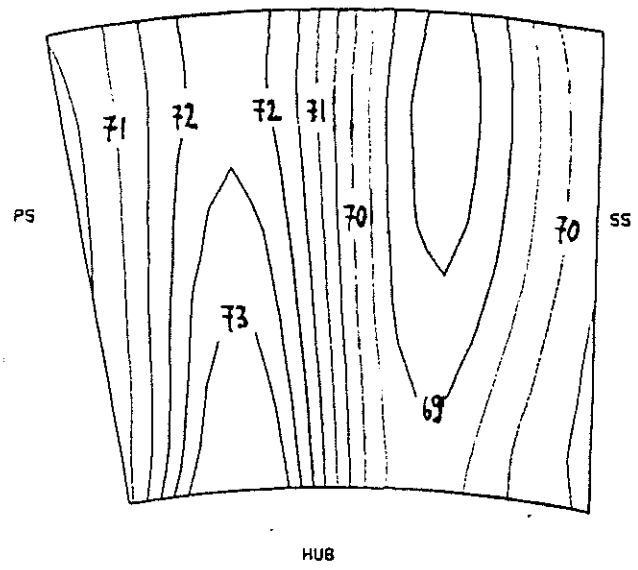

17-b) Test case no. 2

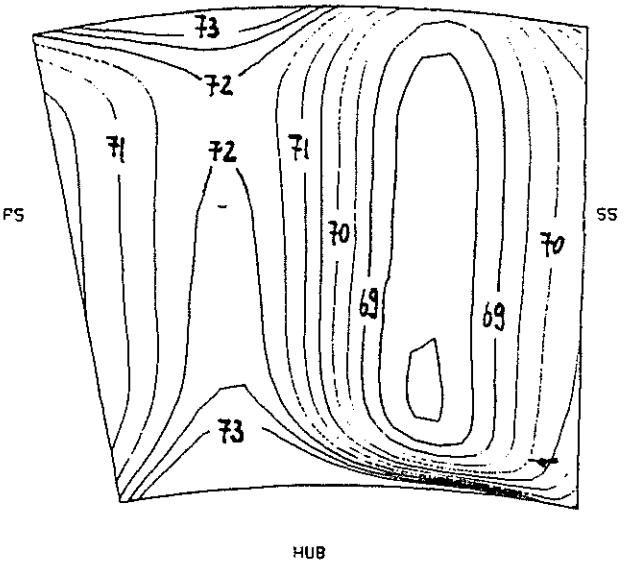

17-c) Test case no. 3

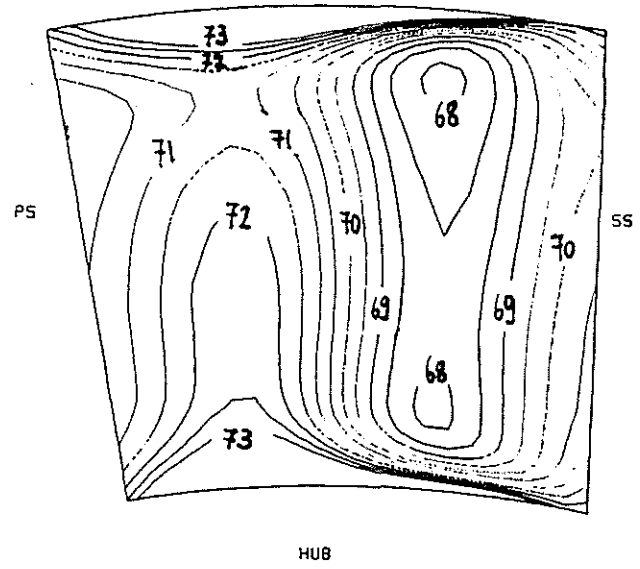

17-d) Test case no. 4

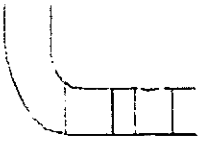

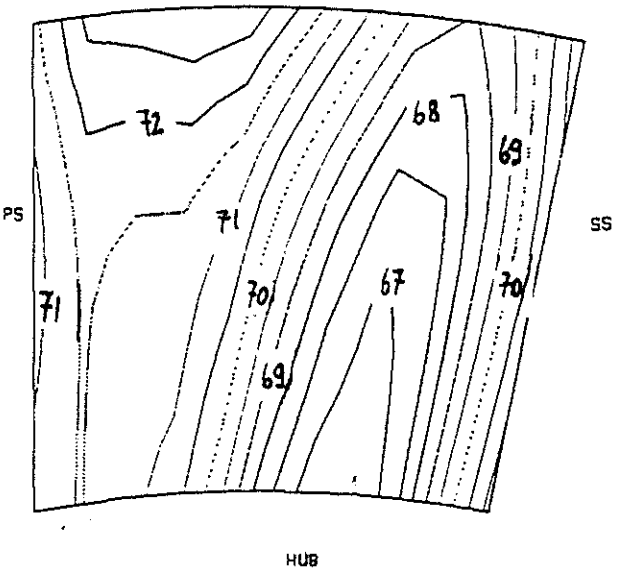

Fig.18 - Laser Two-Focus probe volume

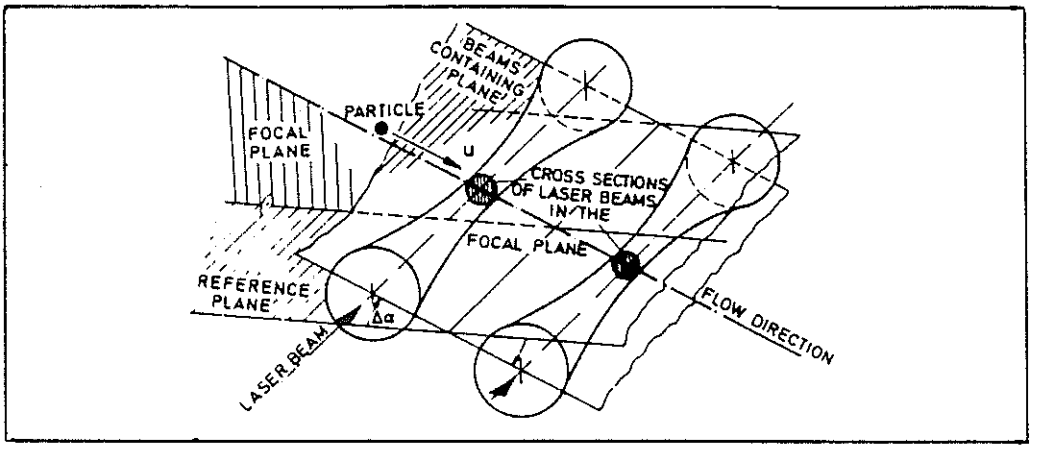

Fig.19 - Laser Two-focus Anemometer optical sistem

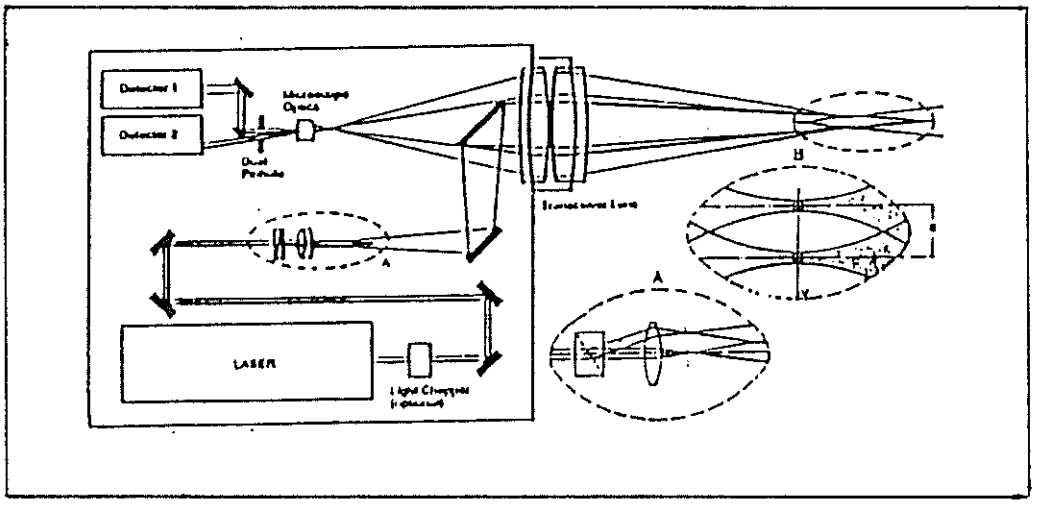

Fig.20 -. Optical Access to L-2-F and measurement plane (1) in the rotor area of the cold-air-turbine rig

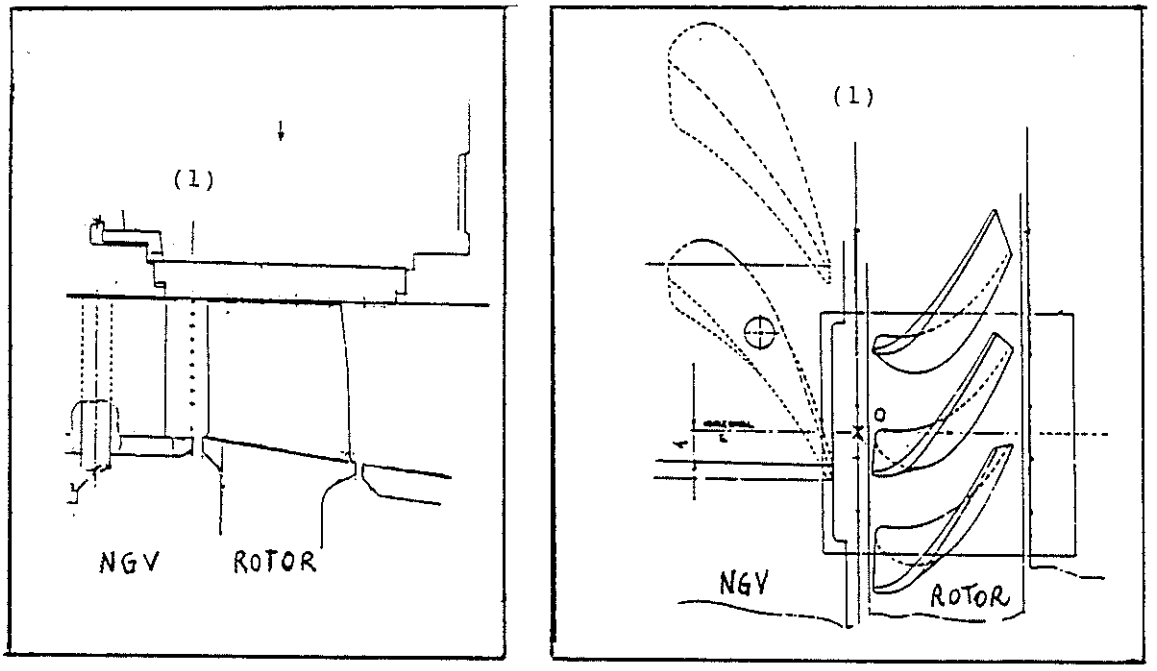

Fig.21/a- Experimental results - NGV Exit Mach Number

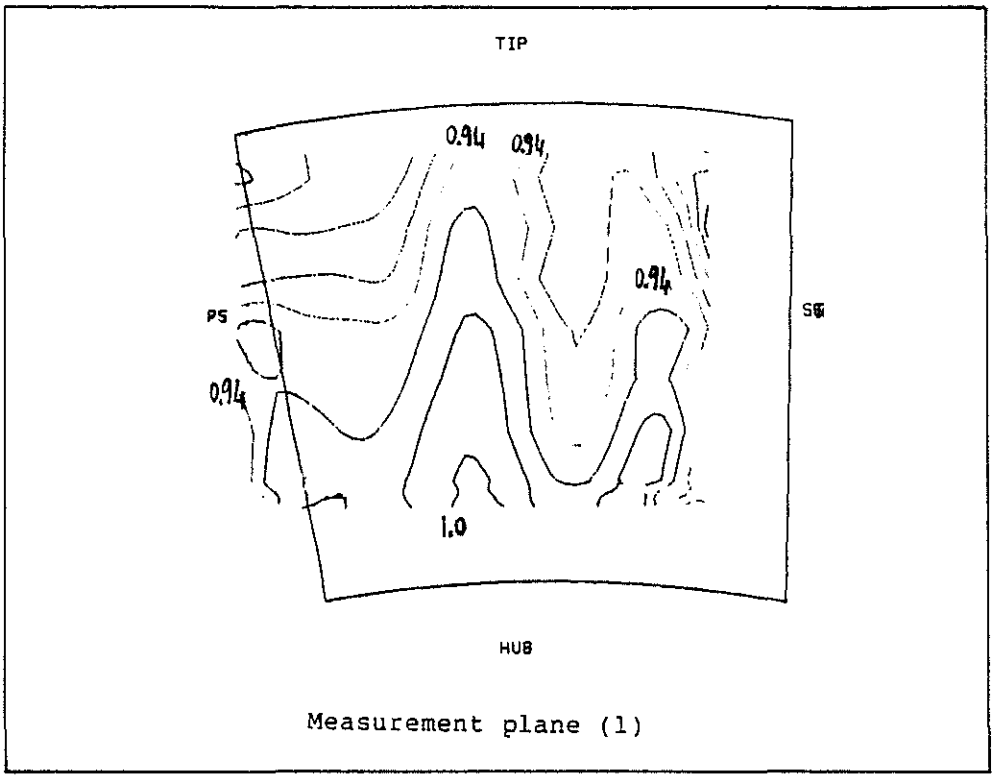

Measurement plane (1)

Fig.21/b- Experimental results - NGV Exit Beta Flow Angle

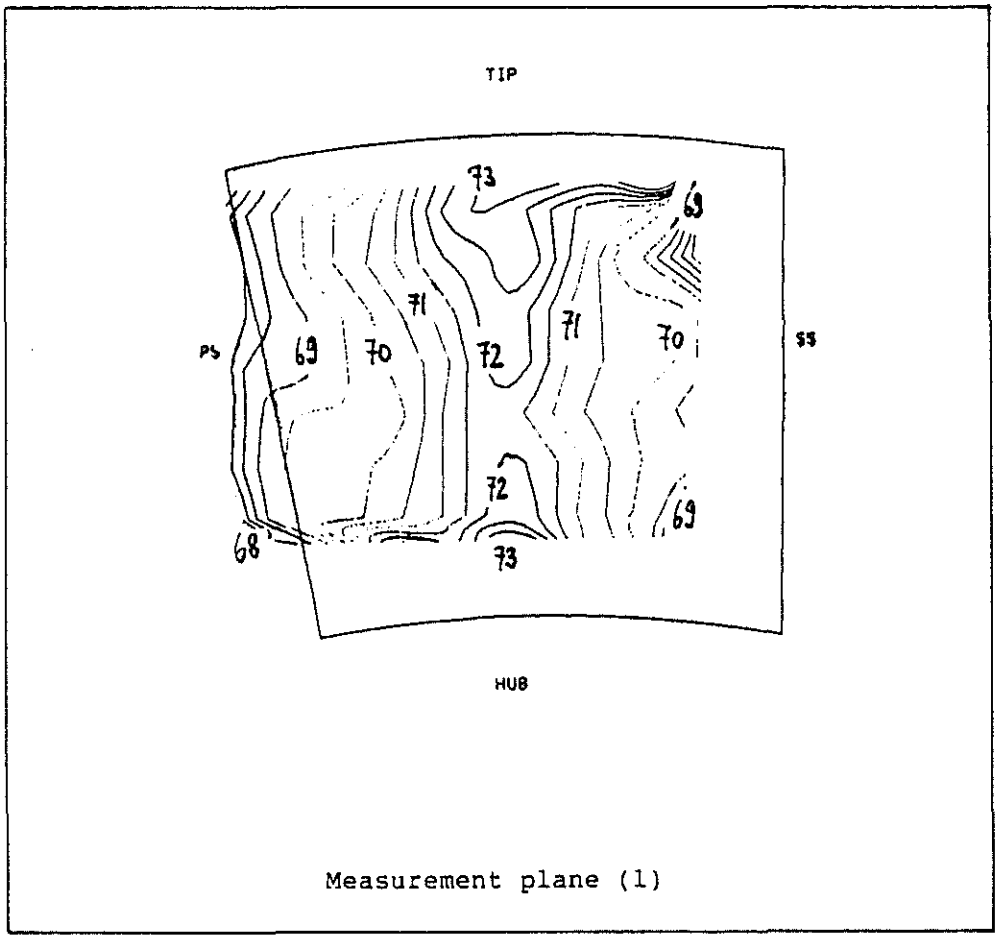

Measurement plane (1)